Applied Clay Science xxx (xxxx) 106276

Contents lists available at ScienceDirect

Applied Clay Science

journal homepage: www.elsevier.com/locate/clay

Antibacterial LDPE-based nanocomposites with salicylic and rosmarinic acid-modified layered double hydroxides

Serena Coiai [a,*], Francesca Cicogna [a], Simone Pinna [a], Roberto Spiniello [a], Massimo Onor [a], Werner Oberhauser [b], Maria-Beatrice Coltelli [c], Elisa Passaglia [a]

[a] Istituto di Chimica dei Composti OrganoMetallici (CNR-ICCOM), SS Pisa, Via Moruzzi 1, 56124 Pisa, Italy
[b] Istituto di Chimica dei Composti OrganoMetallici (CNR-ICCOM), Via Madonna del Piano 10, 50019 Sesto Fiorentino (FI), Italy
[c] Dipartimento di Ingegneria Civile e Industriale, Università di Pisa, Via Diotisalvi 2, 56122 Pisa, Italy

ARTICLE INFO

Keywords:
Layered double hydroxides (LDHs)
Antibacterial molecules
Salicylic acid
Rosmarinic acid
LDPE nanocomposites

ABSTRACT

Polymer nanocomposites, prepared by dispersing layered nanofillers bearing active and natural compounds in a polymer matrix, offer a tunable way to confer antibacterial activity to traditional polymers for packaging materials. Antibacterial host-guest systems were prepared by intercalation of mono-deprotonated rosmarinic and salicylic acid (RA and SA), with recognized antibacterial and antioxidant properties, into a nitrate-intercalated MgAl layered double hydroxide (LDH) *via* anion exchange reaction. The structural, morphological, and thermal properties of the modified LDHs (*i.e.,* MgAl-RA and MgAl-SA), compared with those of a fully exchanged ZnAl-SA, indicated the successful immobilization of the functional molecules. Linear low-density polyethylene (LDPE)/antibacterial-LDH nanocomposites were prepared by a two-step melt compounding procedure. X-ray diffraction analysis and scanning electron microscopy showed that MgAl-RA was better dispersed than ZnAl-SA and MgAl-SA. LDPE nanocomposites containing the highest filler content showed increased thermo-oxidation stability, with a marked effect for LDPE/MgAl-RA due to the antioxidant power of RA. Furthermore, the antibacterial activity of LDPE/MgAl-RA was high and selective toward *Staphylococcus aureus*. Finally, the overall migration of RA and SA from films of polymer nanocomposites immersed in ethanol solution was followed by fluorescence spectroscopy evidencing a controlled release of the active compounds.

1. Introduction

Polymer nanocomposites containing 2D nanofillers have emerged in the past decades as a promising class of materials with improved mechanical, thermal, and barrier performance (Liu et al., 2019; Bhattacharya, 2016; Yue et al., 2019; Fu et al., 2019). Material properties depend not only on the nanosize of reinforcement particles but also on interphase characteristics and interfacial interactions, which dictate matrix chain mobility, filler dispersion and distribution. Much work has been done on the modification of both the filler and the matrix, thus tuning and optimizing the reciprocal interactions and creating a co-continuous organic/inorganic interphase thanks to the improvement of interfacial adhesion (Ciardelli et al., 2008; Ha, 2018).

Today, in addition to optimizing the structural properties of polymer nanocomposites (*i.e.,* mechanical, thermal, rheological), emphasis is given to the introduction of functional features (*e.g.,* bioactive, optical, electrical, sensing, *etc.*). In particular, the 2D geometry of layered nanofillers is beneficial for self-assembly in organized layered structures that can contain functional organic molecules (*e.g.,* dyes, biomolecules, oligomers, stabilizers, *etc.*) (Coiai et al., 2015). These hybrid host-guest systems can be used as fillers for polymers thus obtaining polymer nanocomposites where the structural properties are ruled by the organic/inorganic polymer network and the functional properties are related to the chemical nature of the moieties incorporated into the filler. For example, polymer nanocomposites can be endowed with antimicrobial properties and then used to develop new food packaging materials able to preserve the quality and increase the safety of food products (Gorrasi and Sorrentino, 2020; Bahrami et al., 2020). Antimicrobial agents dispersed into a polymer material extend the product shelf-life by releasing active molecules. However, the heat sensitivity of antimicrobial molecules and fast release from polymeric mixtures, due to poor compatibility, limit their use and development. The encapsulation of antimicrobial agents into nanofillers allows for a controlled release. This effect is maintained even after the dispersion of the encapsulated

* Corresponding author.
E-mail address: serena.coiai@pi.iccom.cnr.it (S. Coiai).

https://doi.org/10.1016/j.clay.2021.106276
Received 28 April 2021; Received in revised form 6 September 2021; Accepted 7 September 2021
0169-1317/

system into a polymeric matrix, suitable for food packaging, thus keeping the food quality over an appropriate timescale (Bahrami et al., 2020).

Among the different inorganic systems that could be used to prepare host-guest systems with antimicrobial agents, layered double hydroxides (LDHs) are one of the most promising. LDHs are a class of anionic clays consisting of positively charged and pillared hydroxide lamellae balanced by hydrated anions intercalated between the layers. The lamellae are made of divalent (Mg^{2+} or Zn^{2+} in the LDHs used here) and trivalent (Al^{3+}) metal cations that are located at the centers of octahedral unit cells with hydroxide ions at the vertices. The interlayer anions can be easily exchanged to produce intercalated systems containing both inorganic and organic anions firmly anchored to the hydroxide layers through ionic bonds (Mishra et al., 2018). The LDHs can then accommodate drugs, bioactive molecules, photofunctional molecules, stabilizers, and catalysts thus covering a variety of application fields (Khan et al., 2009; Xu and Wei, 2018; Taviot-Guého et al., 2018; Coiai et al., 2018). For example, LDHs have been used as nanocarriers of antioxidants like carnosine acid, gallic acid, vanillic acid, ferulic acid, caffeic acid, and many others (Rossi et al., 2005; Kong et al., 2010; Pérez Amaro et al., 2016). In these systems, the intercalation between the layers not only protects the active molecules from oxidation and thermal degradation but also reduces the effects of migration, thus promoting a controlled release over time. Furthermore, the organo-modification of LDH improves the compatibility with the polymer matrix. All these characteristics make LDHs particularly interesting and versatile as additives for polymer composites.

Early reports demonstrated that LDHs can be employed to prepare a variety of antimicrobial host-guest systems (Costantino et al., 2009; Sammartino et al., 2005; Bugatti et al., 2011). For example, antibiotic-intercalated LDHs have been developed preserving the antimicrobial activity of the precursors, improving their thermal stability, and controlling the release kinetics (Ryu et al., 2010; Wang and Zhang, 2012; Li et al., 2019). Bugatti et al. (Bugatti et al., 2013) reported the modification of LDHs with salicylate anions (*i.e.,* o-hydroxybenzoate anions), which have well-known antibacterial properties. In this study, the smaller particles of salicylate-modified LDHs showed faster release kinetics of salicylate molecules and more effective antibacterial activity against *E. coli* than bigger particles. Cheng et al. (Cheng et al., 2019) examined the inclusion of p-hydroxybenzoic acid (PHBA) into LDH. PHBA is, indeed, widely used as a preservative in consumer products, even though its direct contact with food products must be strictly controlled due to its oestrogenic activity. The encapsulation into LDHs improved the safety of PHBA avoiding direct contact with the preserved product and permitting the release by controlled kinetics. Other reports have described the incorporation of these hybrid and antimicrobial systems into a polymer matrix. For example, ZnAl-LDHs intercalated with benzoate and benzoate derivatives were dispersed into poly(ε-caprolactone) (PCL) by high-energy ball milling demonstrating the antibacterial activity of polymer composites *versus Saccharomyces cerevisiae* (Costantino et al., 2009). Similarly, benzoate-LDHs were dispersed into gelatin inhibiting the growth of both *Staphylococcus aureus* and *C. albicans* (Cheng et al., 2019). The collected data evidenced that the functional host-guest systems can slowly release their contents to keep antimicrobial concentrations at the desired levels for a long period time. Similarly, Gorrasi et al. (Gorrasi et al., 2012) described the preparation by ball milling of nanocomposites made of apple peel pectin with 5 wt% of LDH-benzoates. Films of these composites showed antimicrobial activity indicating the potential application as green coating materials in the packaging field.

Nowadays, naturally occurring antimicrobials have gained attention among researchers and food manufacturers due to their safety and non-toxic nature making them a potential alternative to synthetic antimicrobial molecules. For example, essential oils and herb extracts are natural preservatives, which can be used as antimicrobials and food preservative agents and have been also utilized and incorporated into polymeric matrices (Kuorwel et al., 2011; Valdés et al., 2015). Interestingly, phenol-type molecules extracted by olive mill wastewater, which are natural antioxidants and in some cases also antimicrobials, have been confined into the host structure of a ZnAl-LDH, which was used as an integrative filler for the preparation of poly(butylene succinate) (PBS) composites by *in situ* polymerization (Sisti et al., 2019a). The antibacterial properties were assessed against *Staphylococcus aureus* and *E. coli* as representatives of potential agents of foodborne illnesses. Similarly, Sisti et al. (Sisti et al., 2019b) intercalated olive mill wastewater into a ZnAl-LDH to enhance the durability of polypropylene (PP) and PBS melt-blended composites.

Among all the possible natural occurring phenolic molecules with biological activity, rosmarinic acid, an ester of caffeic acid and 3,4-dihydroxyphenyl lactic acid, is a compound commonly found in plants belonging to the Boraginaceae and Lamiaceae, such as rosemary, sage (*Salvia officinalis*), peppermint (Mentha piperita) and thyme (*Thymus vulgaris*) (Veras et al., 2019). It is known for its antioxidant, anticancer, anti-inflammatory, antimicrobial, and antiviral properties (Nadeem et al., 2019). A few reports have described the encapsulation of rosmarinic acid in chitosan, PCL, poly(lactic acid) (PLA) microparticles and polymer gel (Casanova et al., 2016; Kim et al., 2010; Gimenez-Rota et al., 2019) for topical applications. However, to the best of our knowledge the intercalation of rosmarinic acid in LDHs has not been reported yet. The immobilization of rosmarinic acid into a host-guest nanostructured system such as LDHs is convenient not only because it improves the rosmarinic acid stability, and allows for its controlled release, but also because the host-guest system can be dispersed at the nanometer level in a polymer phase. Such a nanocomposite can thus benefit from all the improved thermal, mechanical, and barrier properties provided by dispersed nano-lamellae.

Herein, we report the preparation and characterization of MgAl-LDHs intercalated *via* anion exchange with carboxylate anions of rosmarinic acid (rosmarinate) and salicylate anions (Scheme 1), this latter used for comparison purposes. Both the species possess potential antimicrobial and antioxidant properties that can be transferred to the LDH hybrid system. However, salicylate and rosmarinate anions have

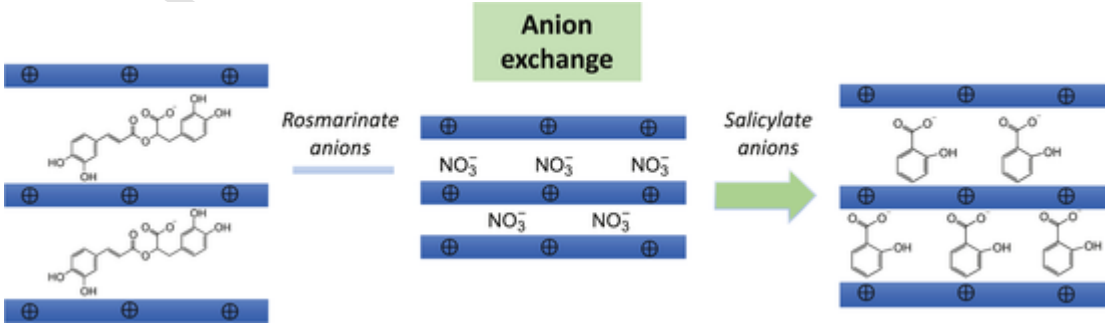

Scheme 1. Schematic representation of anion exchange from a LDH intercalated with nitrate anions with rosmarinate and salicylate anions.

different chemical structures and spatial conformation that can affect the composition, the arrangement of anions between lamellae, and the features of intercalated LDHs. For this reason, although salicylate-modified LDH has already been reported in the literature, here we prepare both salicylate- and rosmarinate-intercalated LDHs under the same operating conditions and we investigate their structural characteristics as well as their ability to be dispersed in a polymer matrix. In addition, the antioxidant and antimicrobial properties of the relative polymer composites are compared.

The structural, spectroscopic, and thermal properties of MgAl-LDHs modified with rosmarinate and salicylate anions (MgAl-RA and MgAl-SA) are determined and compared with that of a ZnAl-LDH intercalated with salicylate anions (ZnAl-SA). Furthermore, dispersion and distribution of MgAl-RA, MgAl-SA, and ZnAl-SA at different percentages into low-density polyethylene (LDPE) by melt compounding is investigated. The dispersion into LDPE of antibacterial-LDHs is indeed of interest to the packaging industry since LDPE is one of the most widely used polymers for flexible packaging. The LDPE-based composites are characterized by X-ray diffraction (XRD) and field emission scanning electron microscopy (FE-SEM) to investigate the morphology and by thermogravimetric analysis (TGA) for assessing the thermal stability. The possible protection toward oxidation of the LDPE matrix due to the dispersion of MgAl-RA, MgAl-SA, and ZnAl-SA is investigated by oxidation induction time (OIT) measurements carried out by differential scanning calorimetry (DSC). Additionally, the antibacterial activity of films of composites is tested against *E. coli* and *Staphylococcus aureus*. Finally, we report a preliminary test for assessing the release kinetics of rosmarinate and salicylate from LDPE/LDH nanocomposites by exploiting the fluorescence emission of rosmarinic acid (Al Danaf et al., 2016) and salicylic acid (Mishra et al., 2004).

2. Materials and methods

2.1. Materials

LDPE, Riblene FL34, with a density of 0.924 g/cm^3 and a melt flow index of 2.1 g/10 min (2.16 kg/190 °C) produced by Polimeri Europa S.p.A (Mantova, Italy) was used in this work. Magnesium aluminum hydroxy carbonate (MgAl-CO_3) Pural MG63HT with the molecular formula $[Mg_{0.66}Al_{0.34}(OH)_2](CO_3)_{0.17}{\cdot}0.62H_2O$ (Coiai et al., 2010) was kindly supplied by Sasol GmbH (Hamburg, Germany). Salicylate zinc aluminum layered double hydroxide (ZnAl-SA) with the molecular formula $[Zn_{0.67}Al_{0.33}(OH)_2](SA)_{0.33}{\cdot}0.50H_2O$ was kindly supplied by Prof. Umberto Costantino's group (University of Perugia, Italy) and used as received. Sodium salicylate (NaSA) (Sigma Aldrich), rosmarinic acid (Sigma Aldrich, 96%), methanol (Sigma-Aldrich), toluene (Sigma-Aldrich, ACS reagent), and chloroform (Carlo Erba, RPE grade), were used as received. Analytical grade chemicals including NaOH, HNO_3 and $NaNO_3$ were used. Deionized ultrapure (Millipore, 18.2 MΩ cm) and free-CO_2 water was used. For the high-performance liquid chromatography (HPLC), acetonitrile and methanol LC-ultraviolet (UV) grade and formic acid ACS reagent grade were used.

2.2. Preparation of MgAl LDH nitrate (MgAl-NO_3), MgAl LDH salicylate (MgAl-SA), MgAl LDH rosmarinate (MgAl-RA)

MgAl-CO_3 was converted into the nitrate form (MgAl-NO_3) according to the titration procedure reported by Muksing et al. (Muksing et al., 2011). 2 g of MgAl-CO_3 were dispersed in 200 mL of $NaNO_3$ 1 M and the suspension was titrated with an HNO_3 1 M until pH = 5. The white solid was recovered by filtration, washed several times with deionized and CO_2-free water, and then dried at 60 °C in a vacuum oven. The calculated anion-exchange capacity (AEC) of MgAl-NO_3 having the formula $[Mg_{0.66}Al_{0.34}(OH)_2](NO_3)_{0.34}{\cdot}0.56H_2O$ (determined according to the analytic procedure described in Muksing et al., 2011) is 3.76 mequiv/g, calculated as follows: AEC = $x/M_w{\cdot}10^3$ (mequiv/g), where M_w and x are the molecular weight and the layer charge per octahedral unit, respectively.

MgAl-NO_3 was converted into MgAl-SA according to the following procedure. A quantity of sodium salicylate (5.64 mmol) corresponding to 1.5 times the AEC of MgAl-NO_3 was dissolved in 50 ml of CO_2-free deionized water. After complete dissolution of sodium salicylate, MgAl-NO_3 (1 g) was added under nitrogen atmosphere and kept in the dark under stirring for 48 h. The solid was recovered by filtration, washed extensively with CO_2-free deionized water, and then dried under vacuum at 60 °C to constant weight.

MgAl-NO_3 was converted into MgAl-RA according to the following procedure. A quantity of rosmarinic acid (5.64 mmol) corresponding to 1.5 times the AEC of MgAl-NO_3 was dissolved in 50 ml of CO_2-free deionized water. Later MgAl-NO_3 (1 g) was added to the solution under nitrogen atmosphere and the suspension with a pH of about 5–6 was kept in the dark and under stirring for 48 h. The pK_{a1} of rosmarinic acid is 2.8–2.9 at which the point of ionization occurs at the carboxylic acid in the 3,4-dihydroxyphenillactic acid moiety, whereas pK_{a2} is 8.4 and the ionization occurs at the *para*-hydroxyl group in caffeic acid (Al Danaf et al., 2016) (Scheme S1, Supplementary Data). At the pH of 5–6, that is the pH of the MgAl-NO_3 suspension containing the solubilized rosmarinic acid, the carboxylate anion of rosmarinic acid is likely the species present in a major amount since this pH corresponds to the first equivalence point of the acid. At the end of the reaction, the solid was recovered by filtration, washed extensively with CO_2-free deionized water, and then dried under vacuum at 60 °C to constant weight.

2.3. Preparation of LDPE/LDH nanocomposites

LDPE/LDH samples, containing 2 and 5 wt% of modified-LDH with respect to the polymer matrix, were prepared (*i.e.,* LDPE/MgAl-SA2, LDPE/MgAl-SA5, LDPE/MgAl-RA2, LDPE/MgAl-RA5, LDPE/ZnAl-SA2, LDPE/ZnAl-SA5). For each type of LDH, two LDPE/LDH master-batches were prepared by mixing 2 g of LDPE and LDH, 80/20 or 50/50%wt, in 30 mL of toluene. The LDPE/LDH toluene solution was sonicated for 20 min with a probe sonicator Hielscher Ultrasonic Processor UP200St (200 W, 26 kHz) equipped with a titanium 2 mm sonotrode S26d2 at the maximum amplitude of 120 μm. The master-batches were isolated through precipitation into methanol, followed by drying under reduced pressure. Later, LDPE/LDH nanocomposites were obtained by diluting the master-batches with LDPE. In a typical experiment, 18 g of LDPE and 2 g of masterbatch (1:10) were added in a Brabender plastograph OHG47055 at 170 °C and mixed at 50 rpm for 10 min. Films of polymer nanocomposites were prepared by compression molding at 170 °C with a Carver press, model 3851–0, and used for analyses.

2.4. Determination of LDH composition

The amount of nitrate anions and organic anions was calculated by ion chromatography and reverse-phase HPLC of solutions obtained after equilibrating 25 mg of LDH in 5 mL of 1 M Na_2CO_3 solution (Table 1). The amount of water in all LDHs was calculated by TGA. The Mg/Al atomic ratio was considered unchanged. On the basis of the values reported in Table 1 a chemical formula for MgAl-NO_3, MgAl-SA, ZnAl-SA, and MgAl-RA was also proposed.

2.5. Characterization

XRD analysis has been performed at room temperature with an X'Pert PRO (PANalytical) powder diffractometer using Ni-filtered Cu Kα radiation (1.541874 Å). All spectra were acquired at room temperature using a Si wafer as a zero background sample holder in the 2θ range between 1.5 and 30°, applying a step size of 0.0131° and a counting time per step of 208 s. The basal spacing of LDHs (d_{003}) was calculated by ap-

Table 1
Quantities of anions and water in LDHs, and LDH molecular formula.

Sample	RA[a] [mg/kg]	SA[a] [mg/kg]	NO_3[a] [mg/kg]	H_2O[b] [wt%]	Molecular formula
MgAl-NO_3	–	–	1234	2.2	$[Mg_{0.66}Al_{0.34}(OH)_2](NO_3)_{0.34}\bullet 0.33H_2O$
MgAl-SA[c]	–	1372	120	8.3	$[Mg_{0.66}Al_{0.34}(OH)_2](SA)_{0.23}(NO_3)_{0.03}(CO_3)_{0.04}\bullet 0.37H_2O$
MgAl-RA[c]	1085	–	120	7.5	$[Mg_{0.66}Al_{0.34}(OH)_2](RA)_{0.11}(NO_3)_{0.09}(CO_3)_{0.07}\bullet 0.72H_2O$

[a] The quantity of RA, SA and NO_3 anions is given as mg of anion per 1 kg of solution. For the test 25 mg of each LDH was put in 5 ml of 1 M Na_2CO_3 solution.
[b] The quantity of water is given as percentage by weight of the hybrid.
[c] The XRD patterns of MgAl-RA e MgAl-SA show a broad reflection around 11.7° of 2θ which can be attributed to the intercalation of carbonate ions occurring during the anion exchange process. In addition, the amounts of RA, SA, and nitrate anions determined by HPLC do not balance the positive charge of lamellae. For this reason, carbonate anions were introduced into the molecular formula.

plying Bragg's law. LDH samples were characterized as powders, whereas LDPE-based nanocomposites as films prepared by compression molding.

Infrared spectra were recorded with a Fourier Transform Spectrometer PerkinElmer Spectrum Two over the wavenumber range of 450–4000 cm^{-1}. The spectra of LDHs were obtained by mixing the sample with potassium bromide (IR-grade KBr, Pike Technologies).

TGA was performed using an Exstar TG/DTA Seiko 7200 instrument. LDH samples (5–10 mg) were placed in alumina sample pans (70 μL) and runs were carried out at the standard rate of 10 °C min^{-1} from 30 to 900 °C under air flow (200 mL min^{-1}). LDPE/LDH composites (5–10 mg) were placed in alumina sample pans (70 μL) and runs were carried out at the standard rate of 10 °C min^{-1} from 30 to 600 °C under nitrogen flow (200 mL min^{-1}) and from 600 to 900 °C under air flow (200 mL min^{-1}).

A Dionex DX-500 ion chromatograph equipped with a GP40 gradient pump and a Rheodyne 7125 injector (25 μL sample loop) was employed for the determination of nitrate content of LDH samples. The nitrate was extracted by equilibrating 25 mg of LDH with 5 mL of 1 M Na_2CO_3 solution for 48 h. The solution was recovered by centrifugation and, before injection, the extracts were filtered through a 0.45 mm Agilent Captiva premium syringe filter. The chromatographic separation was carried out in isocratic mode (flow rate: 1.0 mL min^{-1}; eluent: 2.1 mmol L^{-1} Na_2CO_3 and 0.3 mmol L^{-1} $NaHCO_3$) on a Dionex IonPac AG12 column (4 × 50 mm, 9 μm particle size). Ion suppression was achieved using a Dionex ASRS 300 (4 mm) self-regenerating suppressor in recycling mode. Detection of nitrate was obtained with an AD-20 variable wavelength UV–Vis detector at 215 nm. A Dionex PeakNet chromatography data system (version 4.5) was used for data acquisition and processing. For the calibration of the instrumental response, standard solutions of nitrate were prepared in water and used for the construction of the calibration plot (1, 2.5, 5, 7.5, and 10 mg Kg^{-1} NO_3^-).

The amount of organic anions (rosmarinate and salicylate) in MgAl-SA, ZnAl-SA, and MgAl-RA was determined by HPLC analysis after having equilibrated 25 mg of each type of LDH with 1 M Na_2CO_3 solution for 48 h. The solution was recovered by centrifugation. Before injection, the extracts were filtered through a 0.45 mm Agilent Captiva premium syringe filter. HPLC system 1260 Agilent Technologies equipped with a vacuum membrane degasser, an autosampler and a diode array detector with 60 mm optical length was used. Chromatographic separation was carried out on a Poroshell 120 EC-C18 reversed phase column (4.6 mm i.d. × 100 mm, 2.7 μm particle size, Agilent Technology) with a mobile phase consisting of 95% formic acid (0.1%) and 5% acetonitrile. Analyses were performed in gradient elution conditions 0–10 min: 80% acetonitrile and 20% formic acid (0.1%). Elution was performed at a solvent flow rate of 1 ml min^{-1}. All mobile phase solvents were filtered through a 0.45 μm polyvinylidene fluoride (PVDF) membrane. The column temperature was set at 40 °C and injection volume was 10 μL. UV absorbance was monitored at 340 nm.

FE-SEM analysis on films of LDPE/LDH composites was done using a FEI Quanta 450 FEG scanning electron microscope (Thermo Fisher Scientific, Waltham, MA, USA) (instrument located at CISUP-University of Pisa) equipped with an Everhart-Thornley Detector (ETD) for collection of secondary electrons and a Circular Backscatter Sensor (CBS) for electron-backscatter images. The instrument is coupled to an energy dispersive X-ray spectrometer (EDS). The cryo-fractured surface was covered with a tiny metallic layer of Au, in a way that the surface could be electrically conductive.

OIT measurements were performed using a differential scanning calorimeter DSC 4000 (Perkin-Elmer). The instrument was calibrated by using indium (m.p. 156.6 °C, ΔH = 28.5 J g^{-1}) and zinc (m.p. 419.5 °C). Measurements were performed on disk-shaped specimens with a thickness of 0.20–0.45 mm and weight around 5–10 mg. Samples were isothermally treated at 30 °C under nitrogen flow (50 mL min^{-1}) for 5 min, then they were heated from 30 °C to 200 °C at 20 °C min^{-1} under nitrogen flow (50 mL min^{-1}). After maintaining nitrogen for 5 min to attain thermal equilibrium, the gas was switched to oxygen flow (50 mL min^{-1}). The OIT was determined from the onset of the exothermic oxidation reaction of LDPE shown in the calorimetric curves. Five determinations were done for each sample and the OIT average number was reported.

Fluorescence emission spectra were collected by a FluoroMax4-TCSPC fluorometer (Horiba) with a xenon lamp as the excitation source.

2.6. Antibacterial activity

The *in-vitro* effect of inhibition against *E. coli* and *Staphylococcus aureus* of LDPE/MgAl-SA5, LDPE/ZnAl-SA5, and LDPE/MgAl-RA5 composites was investigated at Laboratory Archa Pisa (Italy) by following the ISO 22196:2011 procedure (Japanese test method JIS Z 2801). Films of composites (40 mm × 40 mm) prepared by compression molding were analyzed and LDPE film was used as control. For each sample, tests were performed in triplicate for the antimicrobial agent. According to ISO 22196:201, the antibacterial activity was evaluated based on the following formula: $R = U_t - A_t$, where R is the antibacterial activity expressed in CFU (number of colony-forming units), U_t is the mean number of bacterial counts obtained from the control sample (CFU/cm^2), and A_t is the mean number of bacterial counts from the surface samples with antimicrobial properties (CFU/cm^2). Data of R are then expressed as log CFU cm^{-2}. The inhibition is considered significant if the antibacterial activity is >2 log CFU/cm^2 (Fontecha-Umaña et al., 2020) and a value of $R \geq 3.07$ log CFU cm^{-2} is considered for both the rules as an indication of complete growth inhibition.

2.7. Migration test

Migration test of salicylate and rosmarinate anions from films of LDPE/MgAl-SA5 and LDPE/MgAl-RA5, respectively, was carried out by putting in contact 100 mg of film (about 100 μm thickness) cut in small pieces with 5 mL of 95% EtOH (EtOH/H_2O 95/5 *v*/v) at room temperature and stirring at 300 rpm. The release kinetics of salicylate and rosmarinate anions was followed by fluorescence spectroscopy. Fluores-

cence emission spectra of solutions were registered at different intervals of time. The excitation lambda was 330 nm in the case of migration test of rosmarinate anions (Al Danaf et al., 2016) and 290 nm in the case of migration test of salicylate anions (Mishra et al., 2004). Blank films of LDPE and rosmarinic acid (LDPE/rosmarinic acid) as well as of LDPE and NaSA (LDPE/NaSA) were prepared by mixing LDPE with 1.5 wt% rosmarinic acid (corresponding to the same amount of rosmarinate anions contained in LDPE/MgAl-RA5 sample) and by mixing LDPE with 1.6 wt% NaSA (corresponding to the same amount of salicylate anions contained in LDPE/MgAl-SA5 sample).

3. Results and discussion

3.1. Rosmarinate (RA) and salicylate (SA)-modified LDHs

RA and SA were intercalated between the lamellae of MgAl-NO_3 upon an anion exchange process (Carlino, 1997). The XRD patterns of MgAl-NO_3, MgAl-RA, MgAl-SA, and ZnAl-SA were acquired and compared (Fig. 1). The XRD profile of MgAl-NO_3 (Fig. 1a) shows the (003) and (006) reflections at 9.9 and 19.8 (2θ). The basal spacing (d_{003}) was 8.9 Å. In the case of ZnAl-SA, the XRD spectrum (Fig. 1b) shows a highly crystalline structure with four distinguishable reflections at 5.5, 11.4, 17.2, and 23.0 (2θ) corresponding to the (003), (006), (009), and (012) reflections, respectively. The basal spacing calculated from the basal peak at 5.5° is 16.0 Å thus demonstrating the effective intercalation of salicylate anions (Costantino et al., 2009). The XRD pattern of MgAl-SA (Fig. 1c) shows broader reflections than ZnAl-SA but positioned at the same 2θ angles. The intercalated structure of MgAl-SA is comparable to that of ZnAl-SA. The broader Bragg reflections of MgAl-SA compared to ZnAl-SA are likely due to a smaller number of pillared layers. However, the increment of the basal spacing demonstrates the successful intercalation of SA. The XRD pattern of MgAl-RA (Fig. 1d) shows a reflection at 4.1° (2θ) likely due to the (003) reflection of the RA-intercalated structure, with a basal spacing of 21.5 Å. The successful intercalation of RA into the LDH structure was also confirmed by a low intense Bragg reflex at 8.2° (2θ) that can be attributed to the (006) reflex of the intercalated structure. However, reflections at 9.9 and 19.8° (2θ) likely due to (003) and (006) reflections of MgAl-NO_3 are still present suggesting a non-quantitative occurred anion exchange, which might be reasonably explained by the higher molecular size of RA compared to SA.

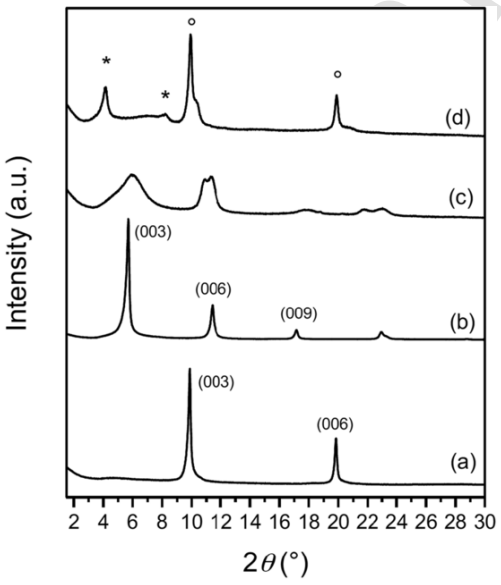

Fig. 1. XRD patterns of (a) MgAl-NO_3, (b) ZnAl-SA, (c) MgAl-SA, and (d) MgAl-RA. Asterisks indicate Bragg reflections originating from MgAl-RA, while circles are assigned Bragg reflections belonging to MgAl-NO_3.

The FT-IR spectra of modified and purified LDHs confirmed the presence of the organo-anions. FT-IR spectrum of MgAl-RA was compared with those of MgAl-NO_3 and sodium rosmarinate obtained by treating rosmarinic acid with a stoichiometric amount of a 0.1 M NaOH solution. The FT-IR spectrum of sodium rosmarinate (Fig. 2c) shows bands at 1688 (νC=C), 1604 (ν_{as}COO), 1525 (νCC), 1446 (νCC, δOH bending in plane), 1384 (νCC), 1264 (νC-OH_{ar}, βOH), 1181 (δCH/νCO)/ 1160 (δCH/δOH), and 1116 cm^{-1} (δCH/δOH) cm^{-1} (Świsłocka et al., 2019). Typical IR bands of RA can be also observed in the FT-IR spectrum of MgAl-RA (Fig. 2b), such as those at 1672, 1590, 1498, 1384, 1266, 1180, 1160, and 1120 cm^{-1}. However, the signal at 1384 cm^{-1} of the MgAl-RA could be also due to the stretching vibration of nitrate groups that remain unexchanged, as evidenced by XRD. Additionally, a band at 670 cm^{-1} due to Mg/Al-OH translation modes (bending vibration) can be observed, which is present also in the spectrum of MgAl-NO_3 (Fig. 2a).

The FT-IR spectra of ZnAl-SA and MgAl-SA, which are compared with those of MgAl-NO_3 and NaSA, show the typical absorption bands of salicylate anion like those at 1600–1606, 1580, 1487, 1460, 1379, and 1254 cm^{-1} corresponding to the asymmetric COO stretching, aromatic ring C—C stretching, symmetric COO stretching, and C—O stretching, respectively (Fig. 3), thus confirming the successful organo-modification. For the sample MgAl-SA, the shoulder at 1360 cm^{-1} could indicate the presence of carbonate anions due to possible nitrate-carbonate exchange that occurred during the preparation or purification steps.

TGA analysis of the modified-LDHs was consistent with the degradation of hydroxide layers and organic anions (Fig. 4). The thermogram of MgAl-NO_3 (Fig. 4a) shows a first step of degradation from 30 to 200 °C due to the dehydration of surface water molecules and to the loss of crystallization water (co-intercalated water and interparticle pore water not totally eliminated during the vacuum drying process) accounting for 7.5% of mass loss of the sample. The second multiple-step from 300 to 600 °C involves the dehydroxylation of the layers and the decomposition of nitrate anions leading to the formation of mixed metal oxides as residue. In the case of MgAl-RA, two main degradation steps can be observed (Fig. 4b). The first step between 30 and 150 °C can be attributed to the loss of water molecules (11.6% of mass loss of the sample); the second step between 150 and 900 °C is the combination of different processes including the dehydroxylation of the layers, the degradation of the rosmarinate anions and even the decomposition of unexchanged nitrate and carbonate anions eventually present. Finally, the thermograms of ZnAl-SA and MgAl-SA (Fig. 4c and d) show a main step with a temperature of maximum degradation rate at about 400 °C that is likely due to the degradation of intercalated salicylate and inorganic anions and to the dehydroxylation of the layers. Multiples steps of degradation are also visible in the range between 30 and 250 °C likely corresponding to the loss of water (7.3 and 9.5 wt%, respectively) and adsorbed organic anions, as previously reported (Frunza et al., 2008). Indeed, the thermal degradation of NaSA takes place in two main steps from 250 to 350 °C (Fig. S1, Supplementary Data) and accordingly the step of degradation from 200 to 250 °C is likely due to salicylate anions adsorbed on the LDH surface.

Chromatographic analysis of solutions containing RA and SA, obtained from known amounts of MgAl-RA and MgAl-SA, respectively, allowed us to calculate the percentage of functional anions which were immobilized between LDH lamellae: 21.7 wt% of RA and 27.4 wt% of SA. Additionally, by combining results obtained from chromatographic analysis and TGA, it has been possible to propose a chemical formula for MgAl-RA and MgAl-SA (Table 1). Differences in the chemical composition of intercalated LDHs can affect the antibacterial and antioxidant properties of the hybrids as well as their dispersion capability and extent of interfacial interactions with the polymer matrix.

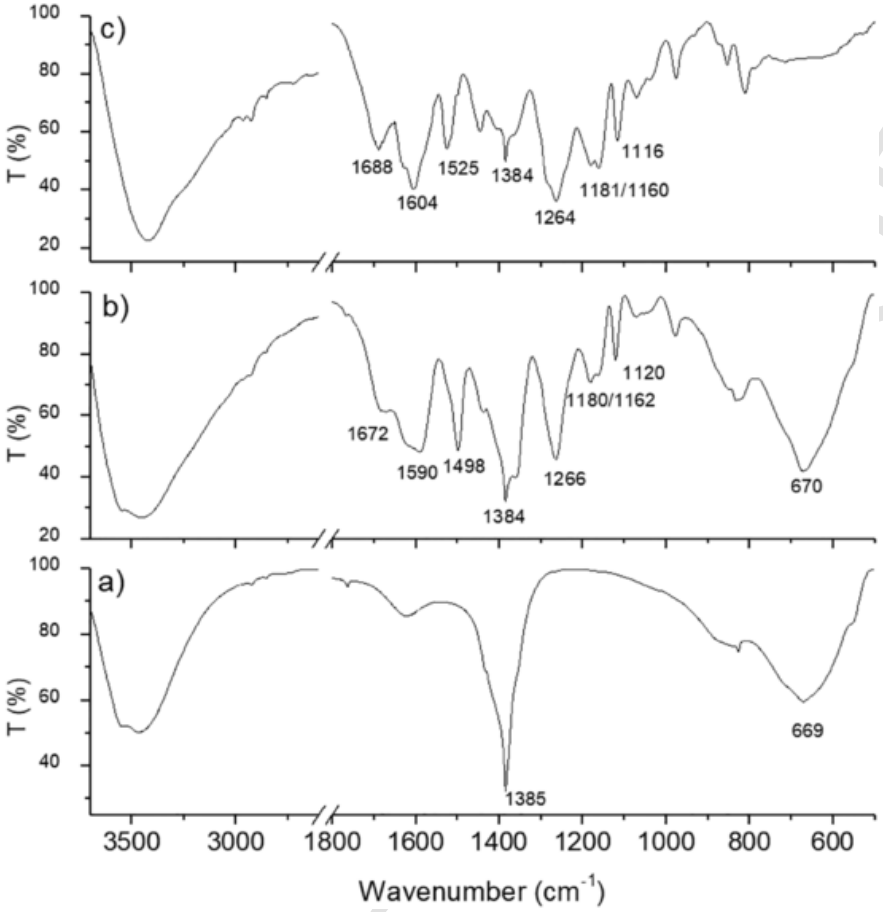

Fig. 2. FT-IR spectra in the regions 3700–2600 and 1800–500 cm^{-1} of MgAl-NO_3 (a), MgAl-RA (b), and sodium rosmarinate (c).

3.2. LDPE/LDH nanocomposites

3.2.1. Structure, morphology, and thermal stability

Fig. 5 shows the XRD patterns of LDPE/LDH nanocomposites (*i.e.,* LDPE/MgAl-SA2, LDPE/MgAl-SA5, LDPE/MgAl-RA2, LDPE/MgAl-RA5, LDPE/ZnAl-SA2, LDPE/ZnAl-SA5) compared with neat LDPE and modified-LDHs. The XRD patterns of LDPE/MgAl-RA2 and LDPE/MgAl-RA5 (Fig. 5a) show reflections of LDPE crystals at 21.5° and 23.5° (2θ), while reflections of MgAl-RA at 9.9° and 19.8° (2θ) are detected only for LDPE/MgAl-RA5, which contained the highest amount of RA. However, these reflections correspond to those of the MgAl-NO_3 fraction still presents in the MgAl-RA, which likely remained as in the original packed assembly. Notably, the reflections of MgAl-RA at 4.1° and 8.2° are not visible for both the composites (LDPE/MgAl-RA2 and LDPE/MgAl-RA5) suggesting that the RA-intercalated fraction of MgAl-RA was well dispersed into LDPE.

The XRD patterns of LDPE/ZnAl-SA composites (Fig. 5b) resulted in a combination of LDPE and ZnAl-SA diffractions. The unchanged position of ZnAl-SA reflections suggests that the intercalated ordinated structure was not fully destroyed by the dispersion in LDPE. However, the XRD pattern of LDPE/MgAl-SA5 does not exhibit readily observable diffraction peaks of MgAl-SA (Fig. 5c) for both compositions (2 and 5%), except for a signal at about 11.6° (2θ) that could be due to a non-organophilic fraction of MgAl-SA. This indicates that MgAl-SA is better dispersed in LDPE than ZnAl-SA owing presumably to its less-ordered starting structure.

To corroborate these findings, FE-SEM micrographs of LDPE/LDH composites with 5 wt% of modified-LDHs were registered on cryo-fractured surfaces. The micrograph of LDPE/MgAl-SA5 acquired with the ETD detector shows a homogeneous morphology of the fracture, but it does not give evidence of the presence of the filler (Fig. 6a). However, using the CBS detector, which collects secondary electrons, it is possible to observe brighter sample zones of micrometric and nanometric size (Fig. 6b) that are agglomerates and nanoparticles of MgAl-SA, as confirmed by EDS analysis (Fig. S2, Supplementary Data).

Micrographs of LDPE/MgAl-SA5 registered with the CBS detector show that the morphology of this sample is generally homogeneous, even though a few big agglomerates of about 10–20 μm can be observed (Fig. 7a). However, by enlarging the homogenous regions, bright particles of nanometric dimension are revealed (Fig. 7b). Similarly, the LDPE/ZnAl-SA5 composite shows a homogeneous morphology in which bright microparticles of the filler are homogeneously distributed into the polymer matrix (Fig. 7d). However, in this case, the dimension of the aggregates (Fig. 7e) is greater than in LDPE/MgAl-SA thus confirming that the LDH dispersion was worse in LDPE/ZnAl-SA5 than in LDPE/MgAl-SA5, in good agreement with XRD results.

LDPE/MgAl-RA exhibits a generally homogeneous morphology, but also in this case agglomerates until 10-μm can be observed (Fig. 7g). However, by enlarging the homogenous regions, numerous bright nanometric particles can be detected (Fig. 7h). Interestingly, the LDH agglomerates are different for the three samples. In particular, in the case of the sample LDPE/MgAl-SA5, the agglomerates show a well-defined layered structure (Fig. 7c) while in the case of LDPE/ZnAl-SA5 the micrometric agglomerates are nanostructured, but a polymeric film seems deposited on them (Fig. 7f). This difficulty in revealing the structure could be an indication of the good interaction with the polymeric matrix. Additionally, for LDPE/MgAl-RA5 the agglomerates seem to strongly interact with the polymer phase (Fig. 7i). In this case, it is hard to distinguish the phase boundary between the polymer and the filler and MgAl-RA seems intimately integrated into the polymer phase sug-

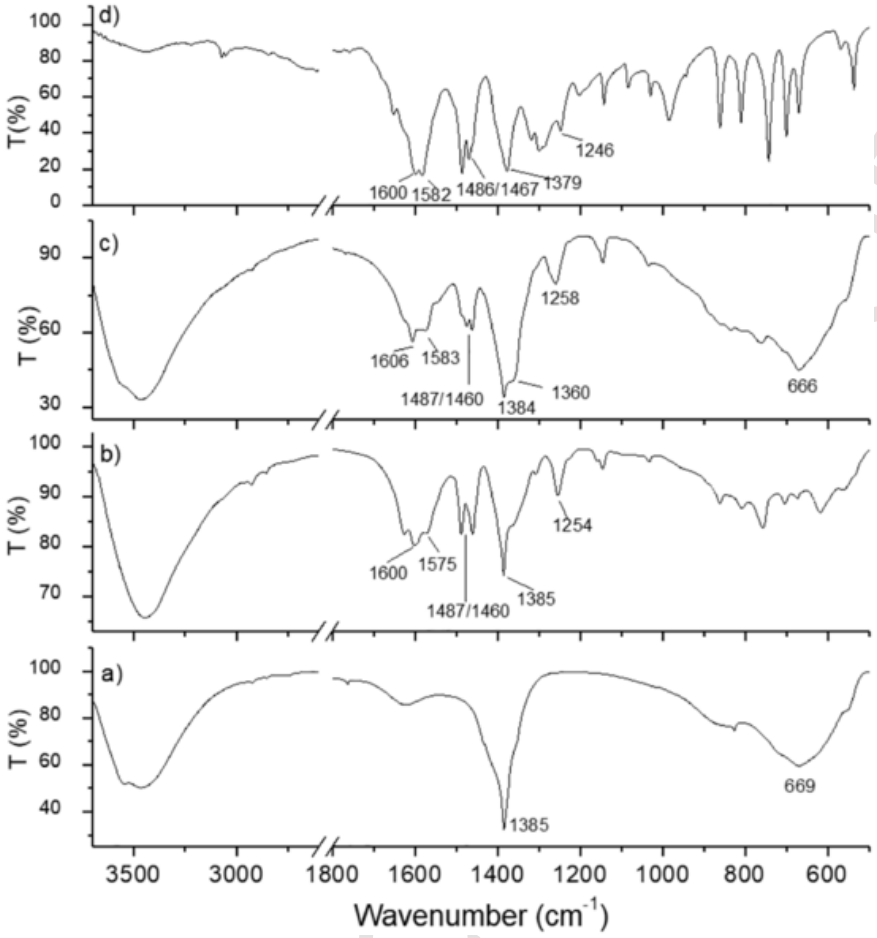

Fig. 3. FT-IR spectra in the regions 3700–2600 and 1800–500 cm^{-1} of MgAl-NO_3 (a), ZnAl-SA (b), MgAl-SA (c), and NaSA (d).

gesting a strong interaction and adhesion (Fig. S3, Supplementary data).

The different levels of dispersion of MgAl-SA, ZnAl-SA, and MgAl-RA into LDPE can perhaps be attributed to the guest-host and guest-guest interactions inside the interlayer region of the hybrid system. Costantino et al. (Costantino et al., 2009) reported that to allow the diffusion of polymer chains inside the interlayer region of a salicylate-LDH, similar in composition to ZnAl-SA, it is necessary to overcome the π-π interactions among the aromatic rings of the intercalated anions and also the network of hydrogen bonds between OH groups of the guest and OH groups of LDH layers. Additionally, ZnAl-SA contains a higher amount of intercalated SA compared to MgAl-SA, making the polymer chain diffusion between lamellae even more difficult. This observation confirms that the dispersion of ZnAl-SA into LDPE is worse than that of MgAl-SA, but the higher amount of intercalated SA in ZnAl-SA probably causes the organic covering of microaggregates observed in FE-SEM images as well as their good interaction with the polymer phase. For MgAl-RA the molecular structure of RA is non-planar thus allowing several possible conformations inside the gallery. Thus, as more conformations are possible and the order on the intercalated anions consequently decreases, a greater possibility to separate the LDH layers by shear stress occurring during the melt mixing and by polymer chains intercalation is expected.

It is worth noting that variations in thermal stability of LDPE nanocomposites compared with neat polymer might affect the range of use and workability of these materials. To investigate this aspect, we characterized LDPE and composites by TGA.

The TGA thermogram of LDPE shows a single step of degradation with T_{onset} (temperature calculated at 5% weight loss) at 424 °C, T_{max} (temperature corresponding to the maximum degradation rate) at 478 °C, and 0.5% mass residue at 900 °C (Fig. 8 and Table S1). All LDPE/LDH nanocomposites are more stable than LDPE showing a slight increase of both T_{max} and T_{onset} with a major increase of 16 °C for the sample LDPE/MgAl-RA2. This result could be explained by either the better dispersion of MgAl-RA as evidenced by FE-SEM and XRD analysis or by the possible greater thermal stability of RA compared to SA. The residual mass at 900 °C was proportional to the amount of inorganic material embedded in all the samples.

3.2.2. *Thermo-oxidation test*

The antioxidant activity of rosmarinic acid and salicylic acid is due to their ability to scavenge hydroxyl radicals by donating hydrogen atoms and it depends on the number of hydroxyl moieties attached to the aromatic ring(s) of the molecules. It has been shown that salicylic acid is a moderate antioxidant and its scavenging activity is lower than gallic acid, caffeic acid, and ferulic acid (Karamac et al., 2005). However, Alamed et al. (Alamed et al., 2009) reported that the free radical-scavenging activity of rosmarinic acid is higher than that of butylated hydroxytoluene, tert-butylhydroquinone, α-tocopherol, and more than three times higher than that of Trolox. It was demonstrated that rosmarinic acid inhibits lipid oxidation in an oil-in-water emulsion (Brewer, 2011) and it can be used to scavenge the surplus of free radicals in the body (Cao et al., 2005). Nevertheless, there is no direct evidence that rosmarinic acid could protect a polyolefin from thermo-oxidation thus replacing synthetic antioxidants. With the OIT test, we investigated the capability of modified-LDHs to prevent the LDPE thermo-oxidation. The resistance of LDPE/MgAl-RA5, LDPE/MgAl-SA5, and LDPE/ZnAl-SA5 against thermally induced oxidation was then

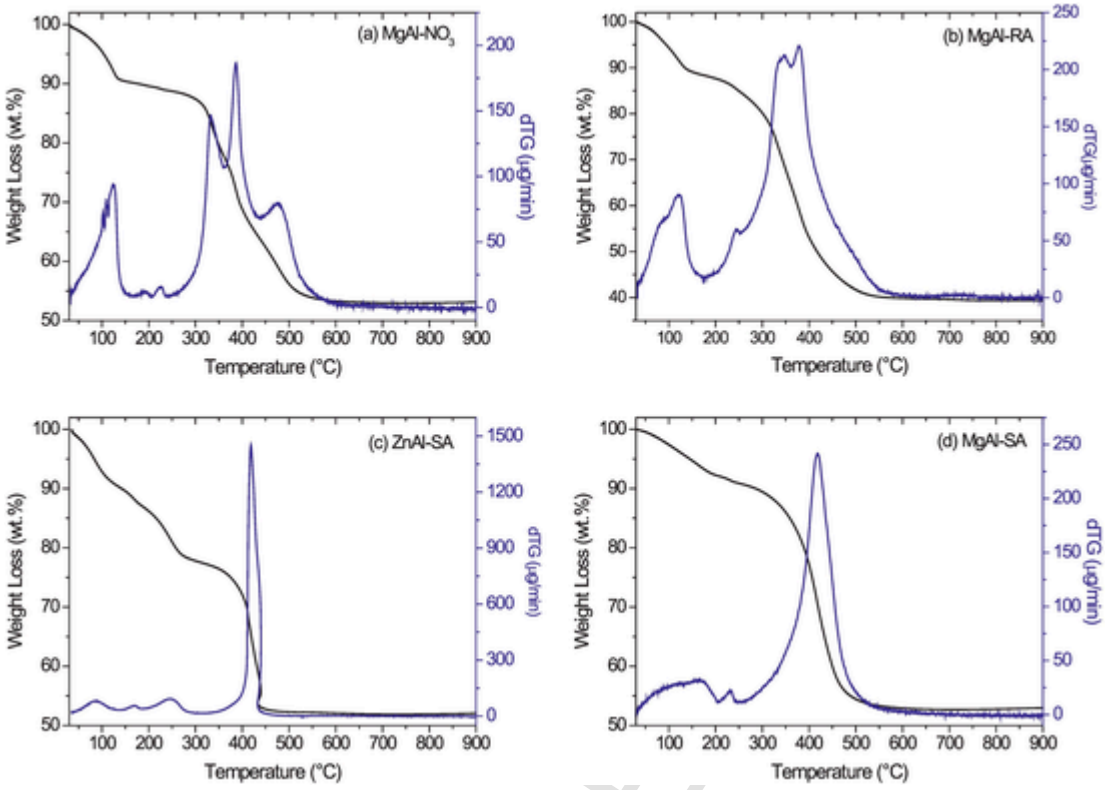

Fig. 4. TGA and DTG curves of MgAl-NO_3 (a), MgAl-RA (b), ZnAl-SA (c), and MgAl-SA (d).

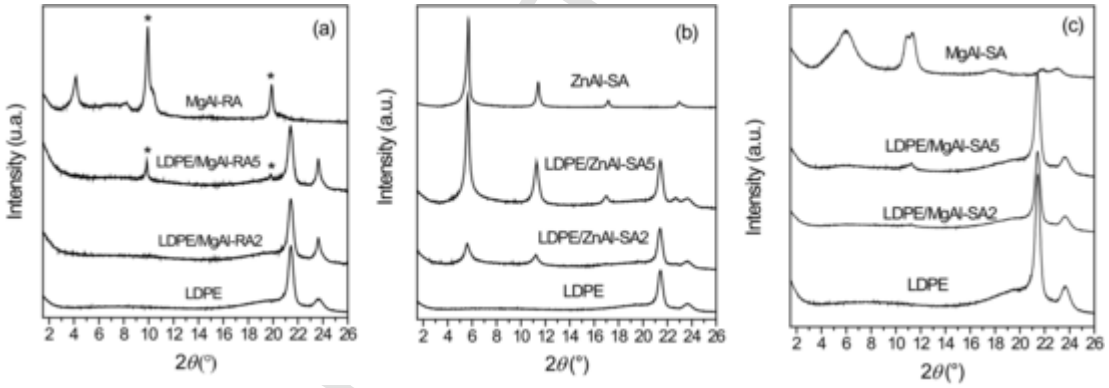

Fig. 5. XRD diffraction patterns of (a) LDPE, LDPE/MgAl-RA2, LDPE/MgAl-RA5, and MgAl-RA; (b) LDPE, LDPE/ZnAl-SA2, LDPE/ZnAl-SA5, and ZnAl-SA; (c) LDPE, LDPE/MgAl-SA2, LDPE/MgAl-SA5, MgAl-SA. Asterisks indicate Bragg reflections originating from MgAl-RA.

evaluated. The OIT is the time that elapses before the sample shows exothermic oxidation during an isothermal experiment carried out under oxygen flow (Fig. 9).

Results show that the oxidation of neat LDPE at 200 °C begins almost immediately, whereas the dispersion of ZnAl-SA, MgAl-SA, and MgAl-RA in LDPE delays the beginning of the polymer oxidative degradation (Table 2).

The effect was most marked in the case of LDPE/MgAl-RA5, which is consistent with the RA chemical structure providing a greater antioxidant capacity than SA. RA has indeed a higher number of hydroxyl groups than salicylate, which can influence the antioxidant mechanism, as previously reported (Quiles-Carrillo et al., 2020). Moreover, the superior antioxidant activity of RA is probably due to the structure of RA where the presence of two aromatic rings with two hydroxyl groups in *ortho*-position would give rise to additional resonance stabilization for the generated phenoxyl radical, and more importantly, could lead to the formation of *ortho*-quinones which are known to act as highly effective chain-breaking acceptor antioxidants (Doudin et al., 2016). It was also observed that the OIT value for LDPE/ZnAl-SA5 was lower than for LDPE/MgAl-SA5 even though the amount of intercalated SA is higher in ZnAl-SA than in MgAl-SA. Possibly, the morphology of the samples and in particular the better dispersion of the LDH layers in LDPE/MgAl-SA5 than in LDPE/ZnAl-SA5 enhanced the stabilization against thermo-oxidation degradation making more available SA.

3.2.3. Antibacterial activity

The antibacterial activity of LDPE/ZnAl-SA5, LDPE/MgAl-SA5, and LDPE/MgAl-RA5 composites was evaluated against two pathogens: the gram-negative *E. coli* and the gram-positive *S. aureus,* which are standard indicators of contamination in the food industry and are capable of adhering, colonizing, and forming biofilms on surfaces. The results of the antibacterial test are shown in Table 3.

The LDPE film has not an antibacterial activity, while sample LDPE/ZnAl-SA5 shows R ≥ 3.07 log CFU/cm^2 for *S. aureus* and $R = 2.78$ log

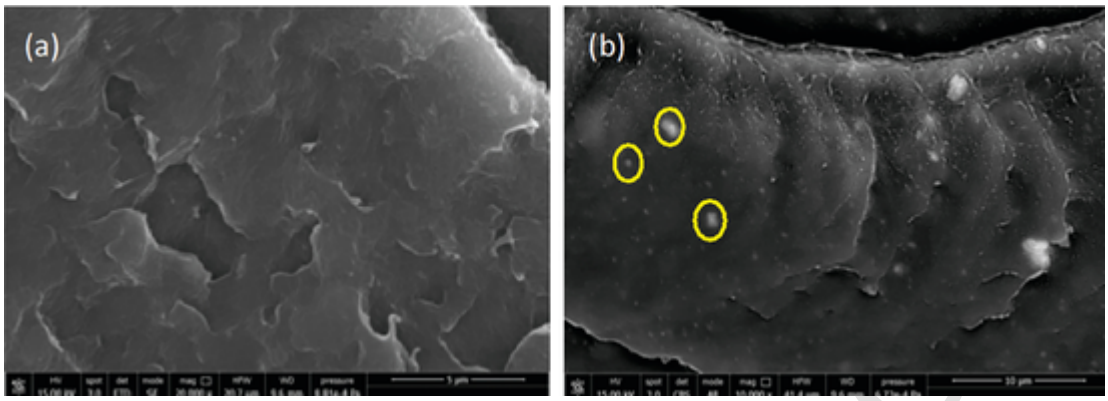

Fig. 6. FE-SEM micrographs registered on the cryo-fractured surface of LDPE/MgAl-SA5: (a) image acquired with the ETD detector and (b) image acquired with the CBS detector.

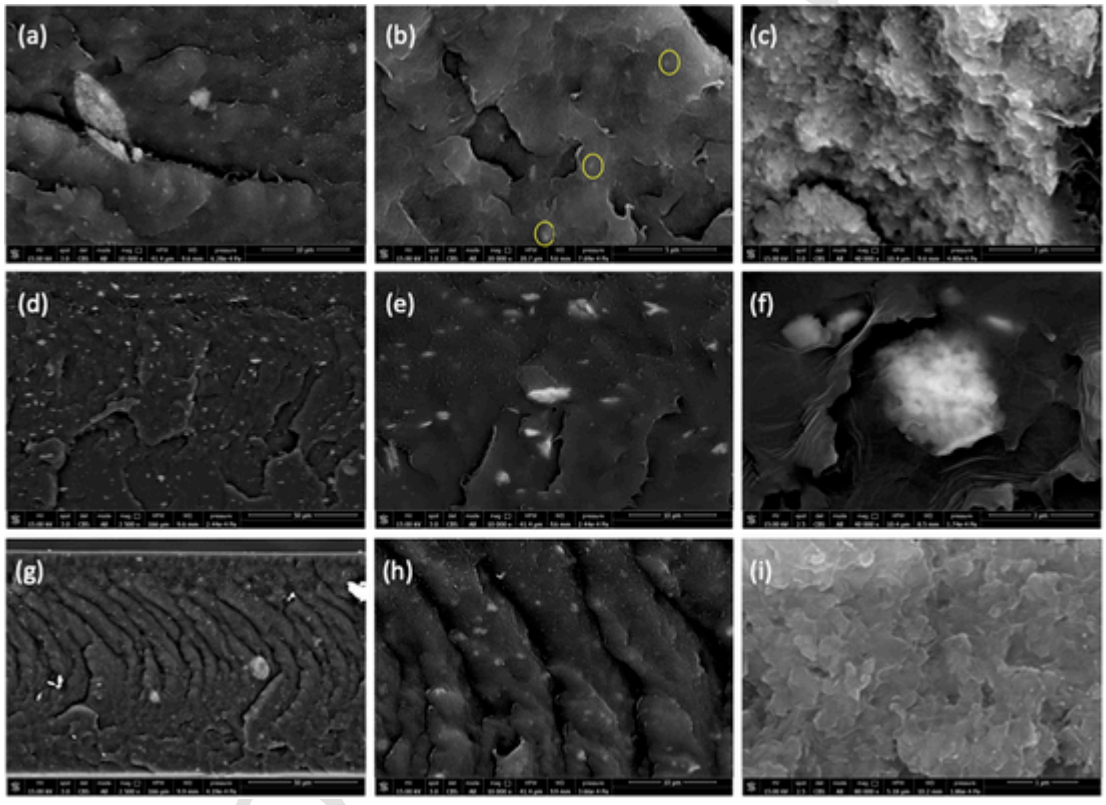

Fig. 7. FE-SEM micrographs obtained with CDS detector for LDPE/MgAl-SA5 (a, b, c), LDPE/ZnAl-SA5 (d, e, f), and LDPE/MgAl-RA5 (g, h, i).

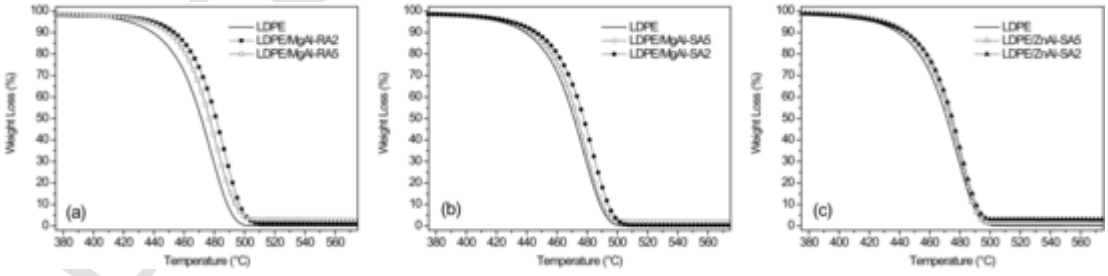

Fig. 8. TGA curves of LDPE/MgAl-RA composites (a), LDPE/MgAl-SA composites (b), and LDPE/ZnAl-SA composites (c).

CFU/cm^2 for *E. coli*. This result demonstrates that ZnAl-SA is strongly inhibitory for both bacteria. However, LDPE/MgAl-SA5 shows only weak inhibition to both bacteria. This different behavior between LDPE/ZnAl-SA5 and LDPE/MgAl-SA5 could be attributed to the presence of Zn(2+) ions in the ZnAl-SA structure. Indeed, the antibacterial activity of zinc oxide is well known. Moreover, ZnAl-SA, as previously reported, could serve as a zinc ion reservoir thus maintaining a high zinc ion concentration (Cheng et al., 2019). Therefore, we speculate

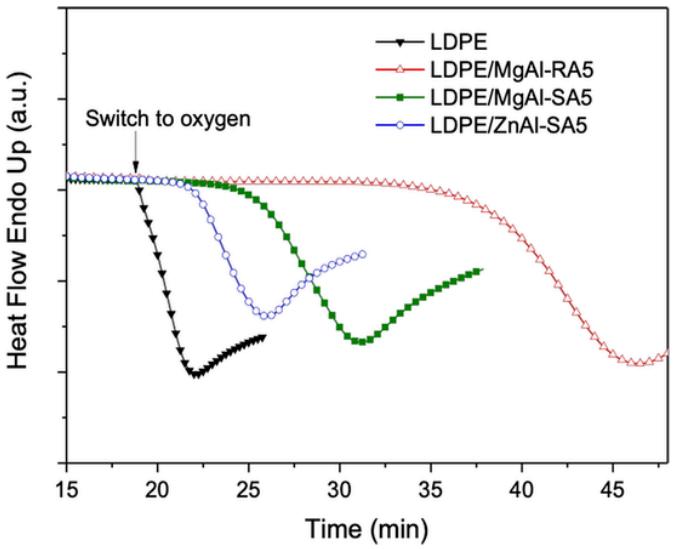

Fig. 9. OIT curves of LDPE, LDPE/MgAl-RA5, LDPE/MgAl-SA5, and LDPE/ZnAl-SA5.

Table 2
OIT values at 200 °C of LDPE, LDPE/MgAl-RA5, LDPE/MgAl-SA5 and LDPE/ZnAl-SA5.

Sample	OIT (min)
LDPE	<1[a]
LDPE/ZnAl-SA5	3.3 ± 0.3
LDPE/MgAl-SA5	7.8 ± 2.7
LDPE/MgAl-RA5	13.9 ± 2.4

[a] The oxidation of LDPE began immediately after the switching of the gas from nitrogen to oxygen at 200 °C.

Table 3
Antibacterial activity (R) of LDPE/ZnAl-SA5, LDPE/MgAl-SA5, and LDPE/MgAl-RA5 against *E. coli* and *S. aureus*. Average of the bacterial counts expressed in log CFU/cm^2.

Sample	Antibacterial activity (R) (log CFU/cm^2)	
	E. coli	*S. aureus*
LDPE/ZnAl-SA5	2.78	≥ 3.07
LDPE/MgAl-SA5	0.73	0.91
LDPE/MgAl-RA5	0.57	≥ 3.07

that the antibacterial activity shown by LDPE/ZnAl-SA is related to the presence of zinc ions. Additionally, the amount of salicylate anions contained in the LDH structure is higher for ZnAl-SA than MgAl-SA (Table 1) thus contributing to the result. Interestingly, LDPE/MgAl-RA was selective and strongly inhibitory toward *S. Aureus*. This result confirms the strong antibacterial activity of RA (Sisti et al., 2019a) and indicates that the LDPE/MgA-RA5 may be used as a highly selective contact-active antibacterial polymer surface.

3.2.4. Preliminary migration test

For an efficient application as a material for active packaging, antibacterial/antioxidant molecules in LDPE nanocomposites need to migrate in a controlled manner when they are put in contact with an extracting fluid. Therefore, we followed the release of RA and SA from films of LDPE/MgAl-RA5 and LDPE/MgAl-SA5 immersed into 95% ethanol, which is a good extracting solvent for both RA and SA, but a non-solvent for LDPE and it is considered a fatty food simulant (Aragón-Gutiérrez et al., 2021). The 95% EtOH solutions containing the released molecules were analyzed by fluorescence spectroscopy (*i.e.*, salicylic acid and rosmarinic acid are indeed fluorescent) (Al Danaf et al., 2016; Mishra et al., 2004) and this property was exploited to qualitatively follow their release from LDPE films. Additionally, a comparison between the release of rosmarinic acid and NaSA directly dispersed into LDPE in a concentration corresponding to that present in the composites was performed. Fig. 10a and c shows the emission spectra of 95% EtOH contact solutions at different time for both LDPE/MgAl-RA5 and LDPE/MgAl-SA5.

The release kinetic of rosmarinate and salicylate molecules ionically bonded to the LDH structure and incorporated into LDPE is also shown for both the samples (Fig. 10b and d) as compared with the release kinetic from the corresponding blank samples (*i.e.,* LDPE/rosmarinic acid and LDPE/NaSA). It is evident that the release of rosmarinate anions from MgAl-RA incorporated into LDPE as well as that of salicylate anions from LDPE/MgAl-SA5 is slower than the release of RA and NaSA simply blended with LDPE. The release of RA and NaSA from blank samples is fast and it reaches the maximum values of intensity after a few hours. Conversely, for LDPE/MgAl-RA5 the release of rosmarinate anions goes on gradually for almost 100 h before reaching a plateau. This is a sought-after behavior in active packaging since it allows to maintain performance for a longer time. Additionally, even though the emission intensity cannot be directly correlated with the fluorophore concentration, the higher intensity observed for blanks is indicative of a major concentration of released RA and NaSA molecules compared to LDPE/LDH composites. Accordingly, the quantity of active molecules that can be released from LDH is lower than the real content in MgAl-RA and MgAl-SA. This result could be due to the incapacity of the solvent to penetrate in depth into the film and accordingly only the layers in contact with 95% EtOH participate to the release of the anions.

4. Conclusions

In summary, we have developed hybrid host-guest systems formed by antibacterial compounds, like RA and SA, intercalated into LDH by anion exchange. To the best of our knowledge, this is the first example of immobilization of rosmarinic acid, a natural antibacterial and strong antioxidant phenolic compound, into a lamellar solid like LDH. The combination of XRD, FT-IR, TGA, and chromatographic data confirmed the intercalation and possible adsorption of RA and SA into MgAl-RA and MgAl-SA which were loaded with up to 22 and 27 wt%, respectively. Even though a commercial rosmarinic acid was used for the experiments, this approach could be further extended to rosmarinic acid extracted from residual biomasses to improve the economic feasibility of the process.

LDPE/LDH nanocomposites containing 2 and 5 wt% of modified LDHs, respectively, were prepared by a two-step procedure consisting of melt blending and compression molding to obtain flexible films. The materials evidenced a general good dispersion of modified LDHs, even though FE-SEM images showed a few micrometric aggregates of LDH particles as a function of LDH concentration and type of functional intercalated anion. A significant effect of stabilization of LDPE thermo-oxidation degradation was observed by OIT-DSC analysis of nanocomposites containing the highest filler content, with a marked effect for LDPE/MgAl-RA5 due to the antioxidant power of RA. Additionally, the antibacterial activity determined by the standard method ISO 22196:2011 for plastic and non-porous surfaces demonstrated that LDPE/MgAl-RA5 was selective and strongly inhibitory toward *S. aureus*, while LDPE/ZnAl-SA5 effectively inhibited the growth of *E. coli* and *S. aureus*, but the effect is likely due to the release of zinc ions. Finally, the overall migration of SA and RA from films of polymer nanocomposites immersed in 95% ethanol solution was followed by fluorescence spectroscopy evidencing a controlled release of the active compounds. The fluorescence emission of nanocomposites is an interesting feature of these materials that could be exploited even for their traceability in packaging applications.

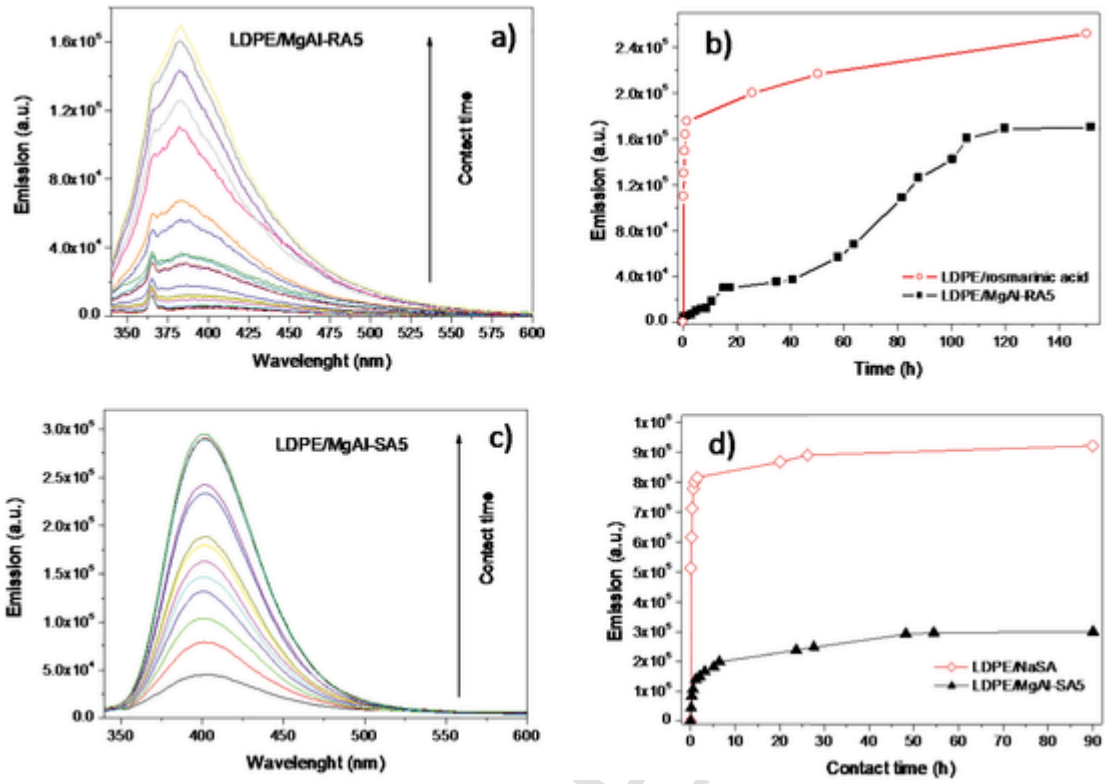

Fig. 10. Fluorescence spectra of 95% EtOH contact solution of LDPE/MgAl-RA5 (a) and LDPE/MgAl-SA5 (c). Release behavior of pure RA from LDPE/RA and LDPE/MgAl-RA5 (b) and of pure NaSA from LDPE/NaSA and LDPE/MgAl-SA5 (d).

CRediT authorship contribution statement

Serena Coiai: Conceptualization, Methodology, Investigation, Data curation, Writing – original draft, Writing – review & editing, Visualization, Supervision, Project administration. **Francesca Cicogna:** Conceptualization, Methodology, Investigation, Data curation, Writing – review & editing, Supervision. **Simone Pinna:** Investigation, Data curation. **Roberto Spiniello:** Investigation. **Massimo Onor:** Investigation. **Werner Oberhauser:** Investigation, Data curation, Writing – review & editing. **Maria-Beatrice Coltelli:** Investigation, Data curation, Writing – review & editing. **Elisa Passaglia:** Conceptualization, Methodology, Investigation, Data curation, Writing – review & editing, Supervision, Resources.

Declaration of Competing Interest

The authors declare that they have no known competing financial interests or personal relationships that could have appeared to influence the work reported in this paper.

Acknowledgements

Scanning electron microscopy was performed using a FEI QUANTA 450 ESEM-FEG at the Centro per la Integrazione della Strumentazione dell'Università di Pisa (CISUP), (https://cisup.unipi.it/). S.C. wishes to thank Dr. Simona Bronco (IPCF CNR Pisa, Italy) for making available the Brabender Plasticorder. Dr. Agostino Bazzichi (Archa Laboratory, Pisa, Italy) is kindly acknowledged for antibacterial activity tests.

Appendix A. Supplementary data

Supplementary data to this article can be found online at https://doi.org/10.1016/j.clay.2021.106276.

References

Al Danaf, N., Abi Melhem, R., Assaf, K.I., Nau, W.M., Patra, D., 2016. Photophysical properties of neutral and dissociated forms of rosmarinic acid. J. Lumin. 175, 50–56.
Alamed, J., Chaiyasit, W., McClements, D.J., Decker, E.A., 2009. Relationships between free radical scavenging and antioxidant activity in foods. J. Agric. Food Chem. 57, 2969–2976.
Aragón-Gutiérrez, A., Rosa, E., Gallur, M., López, D., Hernández-Muñoz, P., Gavara, R., 2021. Melt-processed bioactive EVOH films incorporated with ferulic acid. Polymers 13, 68.
Bahrami, A., Delshadi, R., Assadpour, E., Jafari, S.M., Williams, L., 2020. Antimicrobial-loaded nanocarriers for food packaging applications. Adv. Colloid Interf. Sci. 278, 102140.
Bhattacharya, M., 2016. Polymer nanocomposites-a comparison between carbon nanotubes, graphene, and clay as nanofillers. Materials 9 (4). art. no. 262.
Brewer, M.S., 2011. Natural antioxidants: sources, compounds, mechanisms of action, and potential applications. Compr. Rev. Food Sci. Food Saf. 10, 221–247.
Bugatti, V., Gorrasi, G., Montanari, F., Nocchetti, M., Tammaro, L., Vittoria, V., 2011. Modified layered double hydroxides in polycaprolactone as a tunable delivery system: in vitro release of antimicrobial benzoate derivatives. Appl. Clay Sci. 52, 34–40.
Bugatti, V., Esposito, L., Franzetti, L., Tammaro, L., Vittoria, V., 2013. Influence of the powder dimensions on the antimicrobial properties of modified layered double hydroxide. Appl. Clay Sci. 75, 46–51.
Cao, H., Cheng, W.X., Li, C., Pan, X.L., Xie, X.G., Li, T.H., 2005. DFT study on the antioxidant activity of rosmarinic acid. J. Mol. Struct. (THEOCHEM) 719, 177–183.
Carlino, S., 1997. The intercalation of carboxylic acids into layered double hydroxides: a critical evaluation and review of the different methods. Solid State Ionics 98, 73–84.
Casanova, F., Estevinho, B.N., Santos, L., 2016. Preliminary studies of rosmarinic acid microencapsulation with chitosan and modified chitosan for topical delivery. Powder Technol. 297, 44–49.
Cheng, H.M., Gao, X.W., Zhang, K., Wang, X.R., Zhou, W., Li, S.J., Cao, X.L., Yan, D.P., 2019. A novel antimicrobial composite: ZnAl-hydrotalcite with p-hydroxybenzoic acid intercalation and its possible application as a food packaging material. New J. Chem. 43, 19408–19414.
Ciardelli, F., Coiai, S., Passaglia, E., Pucci, A., Ruggeri, G., 2008. Nanocomposites based on polyolefins and functional thermoplastic materials. Polym. Int. 57, 805–836.
Coiai, S., Passaglia, E., Hermann, A., Augier, S., Pratelli, D., Streller, R.C., 2010. The influence of the compatibilizer on the morphology and thermal properties of polypropylene-layered double hydroxide composites. Polym. Compos. 31, 744–754.
Coiai, S., Passaglia, E., Pucci, A., Ruggeri, G., 2015. Nanocomposites based on thermoplastic polymers and functional nanofiller for sensor applications. Materials 8, 3377–3427.
Coiai, S., Javarone, S., Cicogna, F., Oberhauser, W., Onor, M., Pucci, A., Minei, P., Iasilli, G., Passaglia, E., 2018. Fluorescent LDPE and PLA nanocomposites containing

fluorescein-modified layered double hydroxides and their ON/OFF responsive behavior towards humidity. Eur. Polym. J. 99, 189–201.
Costantino, U., Bugatti, V., Gorrasi, G., Montanari, F., Nocchetti, M., Tammaro, L., Vittoria, V., 2009. New polymeric composites based on poly (ε-caprolactone) and layered double hydroxides containing antimicrobial species. ACS Appl. Mater. Interfaces 1, 668–677.
Doudin, K., Al-Malaika, S., Sheena, H.H., Tverezovskiy, V., Fowler, P., 2016. New genre of antioxidants from renewable natural resources: Synthesis and characterisation of rosemary plant-derived antioxidants and their performance in polyolefins. Polym. Degrad. Stab. 130, 126–134.
Fontecha-Umaña, F., Ríos-Castillo, A.G., Ripolles-Avila, C., Rodríguez-Jerez, J.J., 2020. Antimicrobial activity and prevention of bacterial biofilm formation of silver and zinc oxide nanoparticle-containing polyester surfaces at various concentrations for use. Foods 9, 442.
Frunza, M., Lisa, G., Popa, M., Miron, N., Nistor, D., 2008. Thermogravimetric analysis of layered double hydroxides with chloramphenicol and salicylate in the interlayer space. J.Therm. Anal. Calorim. 93, 373–379.
Fu, S., Sun, Z., Huang, P., Li, Y., Hu, N., 2019. Some basic aspects of polymer nanocomposites: a critical review. Nano Mater. Sci. 1, 2–30.
Gimenez-Rota, C., Palazzo, I., Scognamiglio, M.R., Mainar, A., Reverchon, E., Della Porta, G., 2019. β-Carotene, α-tocoferol and rosmarinic acid encapsulated within PLA/PLGA microcarriers by supercritical emulsion extraction: encapsulation efficiency, drugs shelf-life and antioxidant activity. J. Supercrit. Fluids 146, 199–207.
Gorrasi, G., Sorrentino, A., 2020. Layered double hydroxide polymer nanocomposites for food-packaging applications. In: Thomas, S., Daniel, S. (Eds.), Woodhead Publishing Series in Composites Science and Engineering, Layered Double Hydroxide Polymer Nanocomposites. Woodhead Publishing, pp. 743–779.
Gorrasi, G., Bugatti, V., Vittoria, V., 2012. Pectins filled with LDH-antimicrobial molecules: preparation, characterization and physical properties. Carbohydr. Polym. 89, 132–137.
Ha, C.-S., 2018. Polymer based hybrid nanocomposites; a progress toward enhancing interfacial interaction and tailoring advanced applications. Chem. Rec. 18, 759–775.
Karamac, M., Kosińska, A., Pegg, R.B., 2005. Comparison of radical-scavenging activities for selected phenolic acids. Polish J. Food Nutr. Sci. 14, 165–170.
Khan, A.I., Ragavan, A., Fong, B., Markland, C., O'Brien, M., Dunbar, T.G., Williams, G.R., O'Hare, D., 2009. Recent developments in the use of layered double hydroxides as host materials for the storage and triggered release of functional anions. Ind. Eng. Chem. Res. 48, 10196–10205.
Kim, H.J., Kim, T.H., Kang, K.C., Pyo, H.B., Jeong, H.H., 2010. Microencapsulation of rosmarinic acid using polycaprolactone and various surfactants. Int. J. Cosmet. Sci. 32, 185–191.
Kong, X., Jin, L., Wei, M., Duan, X., 2010. Antioxidant drugs intercalated into layered double hydroxide: structure and in vitro release. Appl. Clay Sci. 49, 324–329.
Kuorwel, K.K., Cran, M.J., Sonneveld, K., Miltz, J., Bigger, S.W., 2011. Essential oils and their principal constituents as antimicrobial agents for synthetic packaging films. J. Food Sci. 76, R164–R177.
Li, M., Sultanbawa, Y., Xu, Z.P., Gu, W., Chen, W., Liu, J., Qian, G., 2019. High and long-term antibacterial activity against Escherichia coli via synergy between the antibiotic penicillin G and its carrier ZnAl layered double hydroxide. Colloids Surf. B: Biointerfaces 174, 435–442.
Liu, Y., Wang, Y., Zhang, C., Liu, T., 2019. 2D nanosheet-constructed hybrid nanofillers for polymer nanocomposites with synergistic dispersion and function. APL Mater. 7 (8). art. no. 080904.
Mishra, H., Misra, V., Mehata, M.S., Pant, T.C., Tripathi, H.B., 2004. Fluorescence studies of salicylic acid doped poly (vinyl alcohol) film as a water/humidity sensor. J. Phys. Chem. A 108 (12), 2346–2352.
Mishra, G., Dash, B., Pandey, S., 2018. Layered double hydroxides: a brief review from fundamentals to application as evolving biomaterials. Appl. Clay Sci. 153, 172–186.
Muksing, N., Magaraphan, R., Coiai, S., Passaglia, E., 2011. Effect of surfactant alkyl chain length on the dispersion, and thermal and dynamic mechanical properties of LDPE/organo-LDH composites. Express Polym Lett 5, 428–448.
Nadeem, M., Imran, M., Aslam Gondal, T., Imran, A., Shahbaz, M., Muhammad Amir, R., Wasim Sajid, M., Batool Qaisrani, T., Atif, M., Hussain, G., Salehi, B., Adrian Ostrander, E., Martorell, M., Sharifi-Rad, J., Cho, C., Martins, N., 2019. Therapeutic potential of rosmarinic acid: a comprehensive review. Appl. Sci. 9, 3139.
Pérez Amaro, L., Cicogna, F., Passaglia, E., Morici, E., Oberhauser, W., Al-Malaika, S., Dintcheva, N.T., Coiai, S., 2016. Thermo-oxidative stabilization of poly(lactic acid) with antioxidant intercalated layered double hydroxides. Polym. Degrad. Stab. 133, 92–100.
Quiles-Carrillo, L., Montava-Jordà, S., Boronat, T., Sammon, C., Balart, R., Torres-Giner, S., 2020. On the use of gallic acid as a potential natural antioxidant and ultraviolet light stabilizer in cast-extruded bio-based high-density polyethylene films. Polymers 12, 31.
Rossi, C., Schoubben, A., Ricci, M., Perioli, L., Ambrogi, V., Latterini, L., Aloisi, G.G., Rossi, A., 2005. Intercalation of the radical scavenger ferulic acid in hydrotalcite-like anionic clays. Int. J. Pharm. 295, 47–55.
Ryu, S.J., Jung, H., Oh, J.M., Lee, J.K., Choy, J.H., 2010. Layered double hydroxide as novel antibacterial drug delivery system. J. Phys. Chem. Solids 71, 685–688.
Sammartino, G., Marenzi, G., Tammaro, L., Bolognese, A., Calignano, A., Costantino, U., Califano, L., Tetè, S., Vittoria, V., 2005. Anti-inflammatory drug incorporation into polymeric nano-hybrids for local controlled release. Int. J. Immunopathol. Pharmacol. 18, 55–62.
Sisti, L., Totaro, G., Bozzi Cionci, N., Di Gioia, D., Celli, A., Verney, V., Leroux, F., 2019a. Olive mill wastewater valorization in multifunctional biopolymer composites for antibacterial packaging application. Int. J. Mol. Sci. 20, 2376.
Sisti, L., Totaro, G., Celli, A., Diouf-Lewis, A., Verney, V., Leroux, F., 2019b. A new valorization route for Olive Mill wastewater: Improvement of durability of PP and PBS composites through multifunctional hybrid systems. J. Environ. Chem. Eng. 7, 103026.
Świsłocka, R., Regulska, E., Karpińska, J., Świderski, G., Lewandowski, W., 2019. Molecular structure and antioxidant properties of alkali metal salts of rosmarinic acid. Experimental and DFT studies. Molecules 24, 2645.
Taviot-Guého, C., Prévot, V., Forano, C., Renaudin, G., Mousty, C., Leroux, F., 2018. Tailoring hybrid layered double hydroxides for the development of innovative applications. Adv. Funct. Mater. 2018 (28), 1703868.
Valdés, A., Mellinas, A.C., Ramos, M., Burgos, N., Jiménez, A., Garrigós, M.D.C., 2015. Use of herbs, spices and their bioactive compounds in active food packaging. RSC Adv. 5, 40324–40335.
Veras, K.S., Fachel, F.N.S., Delagustin, M.G., Teixeira, H.F., Barcellos, T., Henriques, A.T., Bassani, V.L., Koester, L.S., 2019. Complexation of rosmarinic acid with hydroxypropyl-β-cyclodextrin and methyl-β-cyclodextrin: formation of 2:1 complexes with improved antioxidant activity. J. Mol. Struct. 1195, 582–590.
Wang, Y., Zhang, D., 2012. Synthesis, characterization, and controlled release antibacterial behavior of antibiotic intercalated Mg-Al layered double hydroxides. Mater. Res. Bull. 47, 3185–3194.
Xu, M., Wei, M., 2018. Layered double hydroxide-based catalysts: recent advances in preparation, structure, and applications. Adv. Funct. Mater. 28, 1802943.
Yue, X., Li, C., Ni, Y., Xu, Y., Wang, J., 2019. Flame retardant nanocomposites based on 2D layered nanomaterials: a review. J. Mater. Sci. 54, 13070–13105.